SRNL-STI-2009-00596

Key Words:
Waste Tank
Type IV
Stress
Corrosion
Cracking

Retention:
#Permanent#

MECHANISTIC UNDERSTANDING OF CAUSTIC CRACKING OF CARBON STEELS

B. L. Garcia-Diaz
A. K. Roy

30 SEPTEMBER 2009

Savannah River National Laboratory
Savannah River Nuclear Solutions
Aiken, SC 29808

Prepared for the U.S. Department of Energy Under Contract Number DE-AC09-08SR22470

SRNL
SAVANNAH RIVER NATIONAL LABORATORY

DISCLAIMER

Printed in the United States of America

Prepared for
U.S. Department of Energy

DOCUMENT: SRNL-STI-2009-00596

TITLE: **MECHANISTIC UNDERSTANDING OF CAUSTIC CRACKING OF CARBON STEELS**

APPROVALS

_____ Date:_____
B. L. Garcia-Diaz, Author
Materials Performance & Corrosion Technology
Materials Science & Technology

_____ Date:_____
A. K. Roy, Author
Materials Performance & Corrosion Technology
Materials Science & Technology

_____ Date:_____
J. I. Mickalonis, Author
Materials Performance & Corrosion Technology
Materials Science & Technology

_____ Date:_____
B. J. Wiersma, Technical Reviewer
Materials Performance & Corrosion Technology
Materials Science & Technology

_____ Date:_____
K. E. Zeigler, Manager
Materials Performance & Corrosion Technology
Materials Science & Technology

_____ Date:_____
M. E. Maryak, Customer
Structural Integrity Lead & Program Engineering
Liquid Waste Operations

TABLE OF CONTENTS

LIST OF FIGURES

LIST OF TABLES

1.0 SUMMARY

Liquid waste generated by the PUREX process for separation of nuclear materials is concentrated and stored in Type IV single-shell carbon steel tanks at the Savannah River Site (SRS). The Type IV tanks for this waste do not have cooling coils and have not undergone heat treatment to stress-relieve the tanks. After the waste is concentrated by evaporation, it becomes very alkaline and can cause stress corrosion cracking (SCC) and pitting corrosion of the tank materials. SRS has experienced leakage from non-stress-relieved waste tanks constructed of A285 carbon steel and pitting of A212 carbon steel tanks in the vapor space. An investigation of tank materials has been undertaken at SRS to develop a basic understanding of caustic SCC of A285 and A212 grade carbon steels exposed to aqueous solutions, primarily containing sodium hydroxide (NaOH), sodium nitrate ($NaNO_3$), and sodium nitrite ($NaNO_2$) at temperatures relevant to the operating conditions of both the F and H area plants. This report presents the results of this corrosion testing program.

Electrochemical tests were designed using unstressed coupons in a simulated tank environment. The purpose of this testing was to determine the corrosion susceptibility of the tank materials as a function of chemical concentration, pH, and temperature. A285 and A516 (simulates A212 carbon steel) coupons were used to investigate differences in the corrosion of these carbon steels. Electrochemical testing included measurement of the corrosion potential and polarization resistance as well as cyclic potentiodynamic polarization (CPP) testing of coupons. From the CPP experiments, corrosion characteristics were determined including: corrosion potential (E_{corr}), pitting or breakdown potential (E_{pit}), and repassivation potential (E_{prot}). CPP results showed no indications of localized corrosion, such as pitting, and all samples showed the formation of a stable passive layer as evidenced by the positive hysteresis during the scan. Analysis of the CPP data was performed to compare the corrosion susceptibility of the samples under different environmental conditions.

Test results indicated that the most important factors affecting corrosion of the steel are the solution temperature, hydroxide concentration, and the material used in constructing the tanks. Variables that did not significantly affect the corrosion susceptibility of the steel were the nitrate or nitrite concentration and the atmosphere in the tank. The passivation current of the coupons increased exponentially with temperature. Longer-term studies of the passivation current are suggested based on results from the literature for iron in highly caustic environments. Polarization resistance studies showed a significant increase in corrosion rate at 125°C and 12 M hydroxide concentration when compared with tests at lower temperatures and lower hydroxide concentrations. Within the temperature and pH range of these tests, iron oxide, Fe_3O_4, becomes unstable and could account for the increased corrosion susceptibility. The applicability of these conditions should be confirmed and detailed surface studies should be conducted to determine the corrosion resistance of A285 and A516 carbon steels under these conditions. Surface science studies should also be conducted to determine the role of the carbon steel composition in preventing corrosion under these conditions.

2.0 INTRODUCTION

2.1 PROJECT BACKGROUND

Radioactive liquid wastes, generated from reprocessing of nuclear fuel, have been stored in Type IV single shell tanks since the 1960's. These tanks are located in the F and H areas at the Savannah River Site. The F-area plants used the Purex process involving separation of plutonium (Pu) from uranium (U) metal targets. On the other hand, the separation process used in the H-area plants, was aimed at recovering enriched U from aluminum-U alloy fuel. Nevertheless, both processes involved nitric acid dissolution of fuel and targets containing radioactive fission products, followed by solvent extraction of products. The resultant acidic wastes were subsequently made basic through addition of sodium hydroxide (NaOH) prior to their transfer to the tank farms.

The F-area contains four Type IV tanks, Tanks 17-20F, while four additional tanks, Tanks 21-24H, were subsequently built in H-area. Leaks had been reported through the steel-liners of Tanks 19 and 20 in F-area during the 1980's.[1] There are indications that leakage through the F-tanks could be the result of stress corrosion cracking (SCC) of the carbon steel (A285) used in their construction.[1, 2] Even though the liner material (A212) of the H-tanks has so far exhibited no leaks through their walls, slight pitting tendency has been observed in Tank 23H, which has been attributed to vapor-space corrosion. In general, it has been anticipated that A212 steel may not suffer from either nitrate or caustic SCC due to differences in its chemical composition and metallurgical microstructures.

This investigation is primarily focused on the development of a basic understanding of SCC phenomenon of both carbon steels (A285 and A212) as functions of both metallurgical and environmental variables relevant to the operating conditions of both F and H-area plants. A comprehensive test matrix has been proposed that will enable the determination of plausible causes of failure of the tank structural materials that will eventually lead to the mitigation of environment-induced degradation. A series of electrochemical tests have been designed to provide insight into the corrosion behavior of the tank steels in caustic environments. Further, the role of dissolved gases on the cracking tendency of these steels will be evaluated.

2.2 LITERATURE REVIEW ON CAUSTIC CRACKING

Investigations of the properties of iron and alloys under conditions similar to those in the Type IV waste tanks can provide insight into the electrochemical behavior and possible corrosion mechanisms of the tank materials. Examples include caustic cracking of pressure vessels that have been reported during alumina processing (Bayer process) and pulp-and-paper processing (Kraft process).[3] Also, the use of an iron electrode in a highly basic solution had been proposed by Edison near the turn of the century for use in batteries.[4]

Early literature studies of iron based materials in caustic solution focused on identifying the reaction products and mechanisms due to the oxidation of an iron electrode.[4-8] However, the electrochemical experiments performed in these literature studies[4-8] give insight into the state of the alloy surface when exposed to caustic solutions and the electrochemical reactions occurring within different potential ranges. Surface studies, focused on the reaction of iron electrodes,[5, 7, 8] found that during oxidation of the electrode, two distinct phases occur. In these studies, the iron electrode was oxidized at a constant current of 1 mA after being

charged at -1.1 V for 5 minutes to get a reproducible surface. Figure 1 shows the electrode potential during a constant current oxidation of an iron electrode.

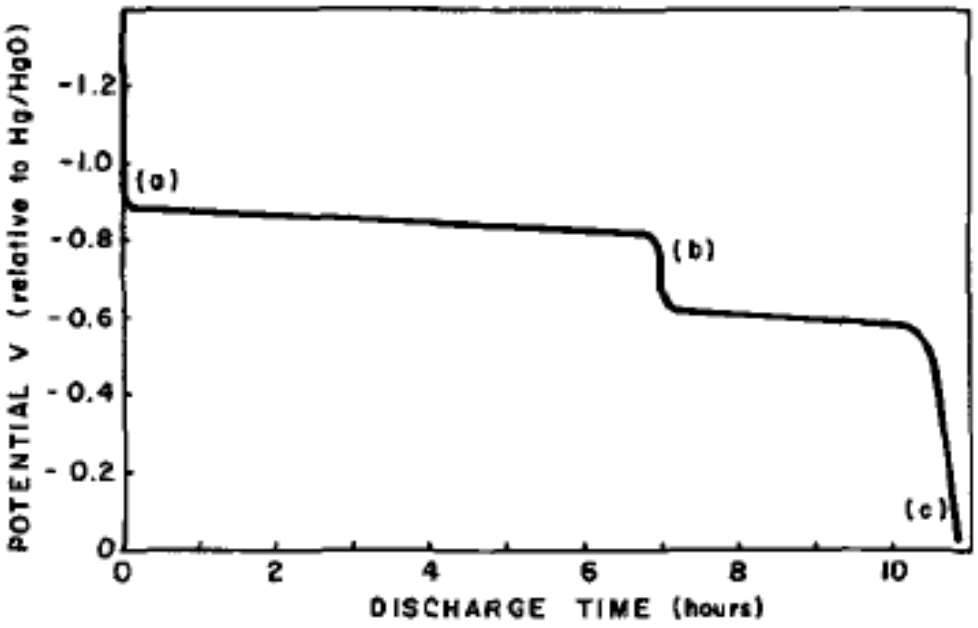

Figure 1. Constant current oxidation of an iron electrode 25°C in 30% KOH[8]

SEM[7] and X-ray diffraction[8] studies of the surface of the oxidized sample showed the iron surface was oxided to form $Fe(OH)_2$ crystals on the surface, as indicated by the first plateau. Subsequently, these crystals were further oxidized to form iron oxyhydroxide, FeOOH, and was then converted to Fe_3O_4. The chemical reactions associated with the formation of FeOOH are shown below.

$$Fe + 2OH^- \leftrightarrow Fe(OH)_2 + 2e^- \quad E^0_{25°C} = -0.917V$$

$$Fe(OH)_2 + 2OH^- \leftrightarrow Fe_3O_4 + 4H_2O + 2e^- \quad E^0_{25°C} = -0.907V$$

$$Fe(OH)_2 + OH^- \leftrightarrow FeOOH + H_2O + e^- \quad E^0_{25°C} = -0.805V$$

The combination of these reactions produces a characteristic pattern during cyclic voltammetry (CV) experiments of the electrodes around room temperature. Figure 2 shows the initial CV scan for an iron electrode in a LiOH solution and the stable CV scan in the same solution after 10 cycles.

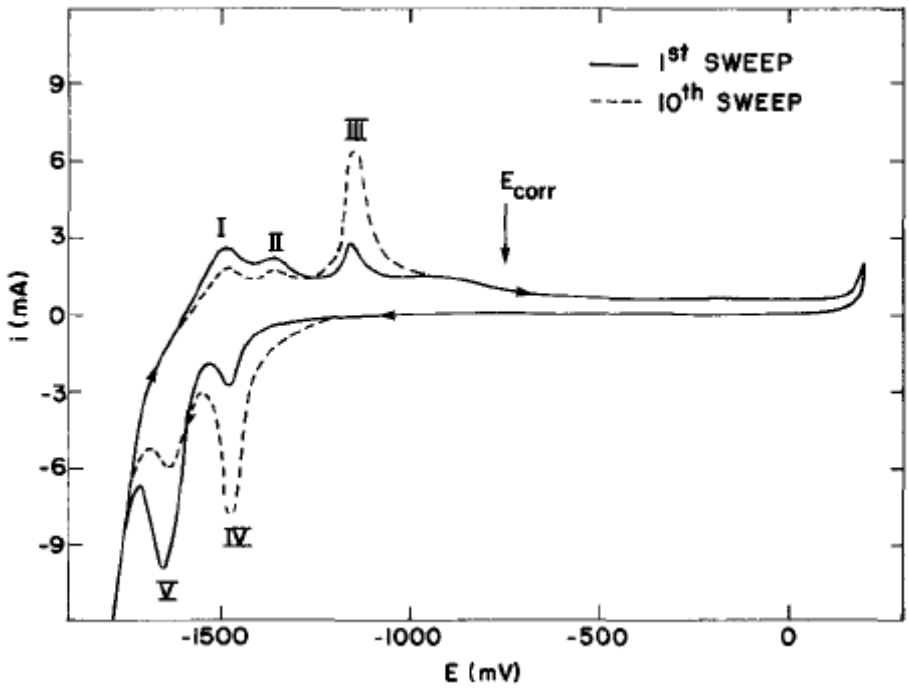

Figure 2. Cyclic voltammetry sweeps of an iron electrode in a 1 M LiOH electrolyte at room temperature[6]

During the development of the stable profile, peaks III and IV in Figure 2 exhibited increases in current while the other peaks showed decrease. By reversing the CV at different potentials, a correlation of the oxidation and reduction peaks in these scans were determined, as shown in Figure 3. Zhang and Park[9] used this analytical technique to determine the oxidation mechanism for the reaction on the iron electrode at room temperature and correlated the peak currents to the reaction mechanism shown above. These results may provide a basis to develop an understanding of electrochemical reactions of iron in highly alkaline solutions at elevated temperatures.

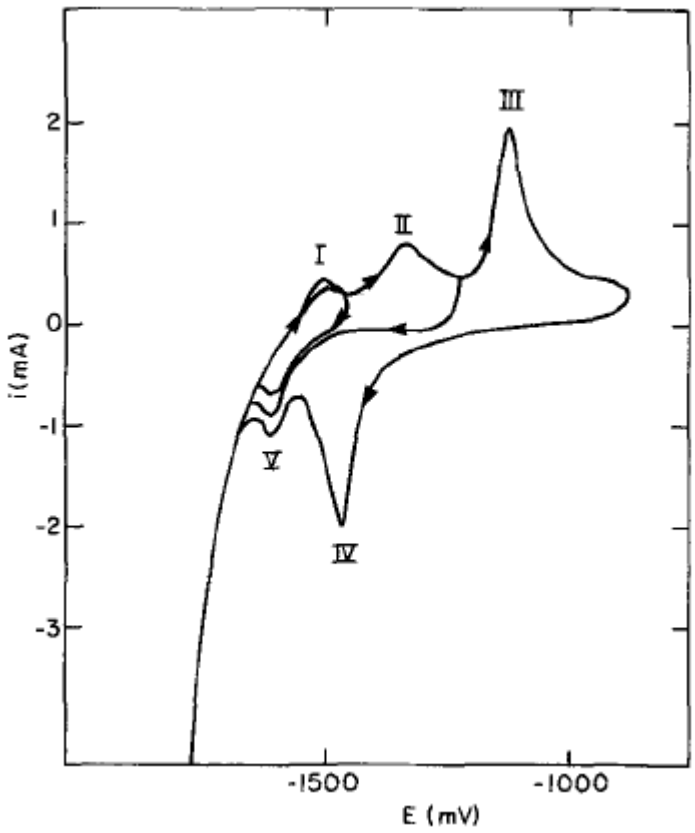

Figure 3. Cyclic voltammagrams of an iron electrode at room temperature that were reversed at different potentials

An interesting aspect of these electrochemical data is how they change with increased temperature. Wieckovski et al.[10] studied A516 steel to understand the damage to pressure vessel walls during the Bayer process. They noted peaks III and IV in a CV scan similar to those shown in Figure 3 disappeared at temperatures above 65°C while peak II increased significantly. They also noted that SCC was not evident at temperatures below 65°C. Therefore, the reaction mechanism at temperatures below 65°C helped to prevent crack initiation. Figure 4 [10] shows CVs for an iron electrode at temperatures between 45 and 95°C. These data show growth in peak II and a decrease in peak III with temperature. These authors also noted that at temperatures above 65°C the steady state CV profile was not significantly different from that of the initial CV. The transition in the reaction mechanism at 65°C also coincided with a change in slope in the "Reduction of Area" versus "Temperature" plots for A516 steel during slow strain rate testing.[10] The results of the slow strain rate testing are shown in Figure 5.[10] Nevertheless, a shift in the electrochemical behavior of the tested coupons appears to indicate a transition in the reaction mechanism that could enhance the material's susceptibility to SCC.

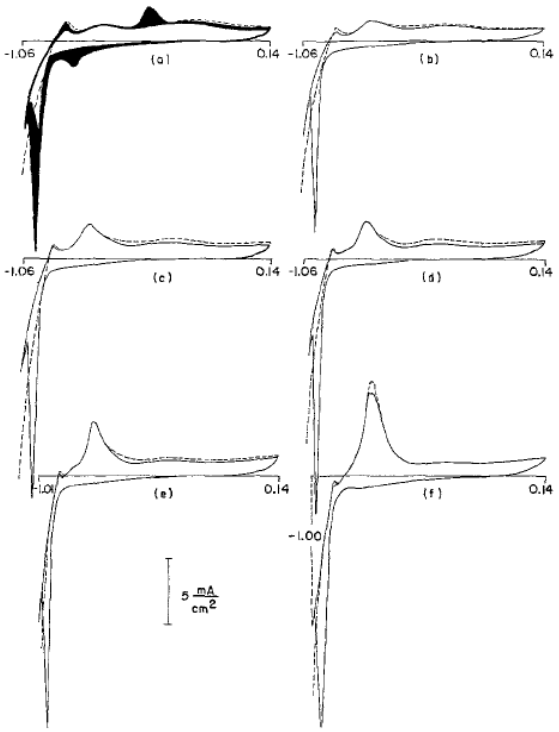

Figure 4. Cyclic Voltammograms of an iron electrode in 1 M NaOH at (a) 45°C, (b) 55°C, (c) 65°C, (d) 75°C, (e) 85°C, and (f) 95°C. Scan Rate: 50 mV/s. [10]

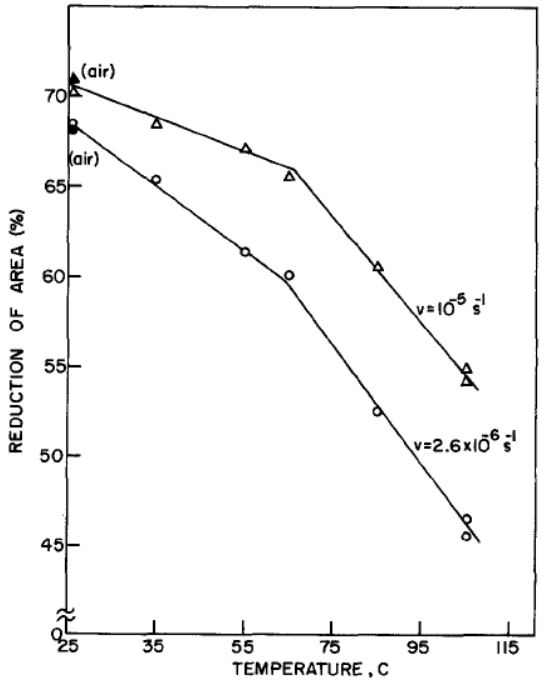

Figure 5. Slow-strain rate reduction of area results for A516 stainless steel in a solution with 7.7 M sodium hydroxide.[10]

Figure 6 shows constant oxidation potential plateaus during 1 mA constant current oxidation experiments at temperatures ranging from 0°C to 70°C.[5] The sustained oxidation potential of steels increased with the reaction temperature.

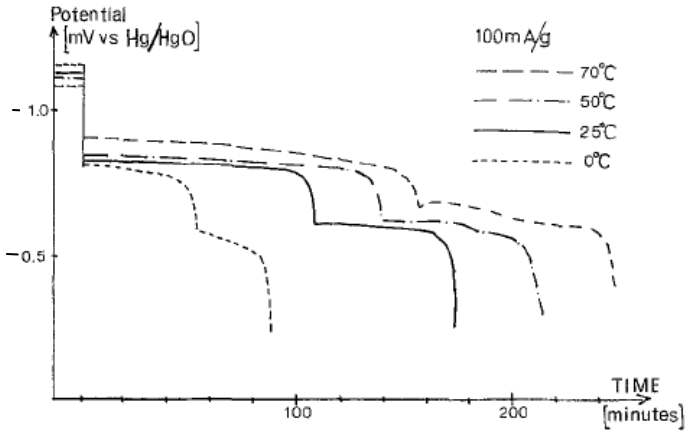

Figure 6. Constant current oxidation of iron electrodes at various temperatures.[5]

The oxidation curves in Figure 6 show that the reaction voltage was shifted to more negative values as the temperature was increased. This is predicted by the general thermodynamic trends as shown in Table 2 in the results section. Another interesting aspect of the oxidation potential profiles was that at higher temperatures the electrodes took longer time to increase potential and passivate. Therefore, the potentials in higher temperature experiments would stay active longer before forming a passive layer that would increase the electrode potential. Discussion by MacDonald and Owen[6] indicated that higher temperature studies provided experimental results that were more reproducible. The more rapid formation of a passive layer on the metal surface at low temperatures could lead to decreased reproducibility of experimental data.

3.0 MATERIALS AND EXPERIMENTAL PROCEDURE

3.1 MATERIALS

Materials tested in this investigation are two types of carbon steels, A285 (UNS K02200) and A516 (UNS K01800). A516 was used instead of A212 since it has recently been replaced by A516. The maximum carbon content in these steels was 0.22 and 0.26 weight percent (wt %), respectively. They were procured from a qualified vendor in quenched and tempered conditions. The chemical compositions and the mechanical properties of the as-received coupons were vendor certified.

3.2 EXPERIMENTAL PROCEDURE

The susceptibility of carbon steels to localized corrosion (pitting/crevice) in aqueous solutions that simulate the tank environment was evaluated by using the CPP technique, according to the test matrix shown in Table 4 in Appendix A. The variables tested include: varying oxygen and nitrogen ratios; varying the concentrations of nitrate, nitrite and hydroxide; and varying the solution temperature. Other chemical species that were included in the simulated solutions are given in Table 5 in Appendix. A three-electrode polarization method involving a working electrode (test specimen), a reference electrode (Hg/HgO), and

graphite counter electrode was used in CPP testing. A potential scan rate of 0.17 mV/sec was used. The magnitude of the corrosion potential (E_{corr}), critical pitting potential (E_{pit}), and protection potential (E_{prot}) were determined from the CPP testing. Experimental testing procedures have been described in previous publications.[11]

4.0 RESULTS AND DISCUSSION

4.1 EXPERIMENTAL RESULTS

Figure 7 shows the surface of an as-received A285 testing coupon before electrochemical testing. The surface of the sample was not modified before testing. The sample surface has lines in the direction of the surface milling.

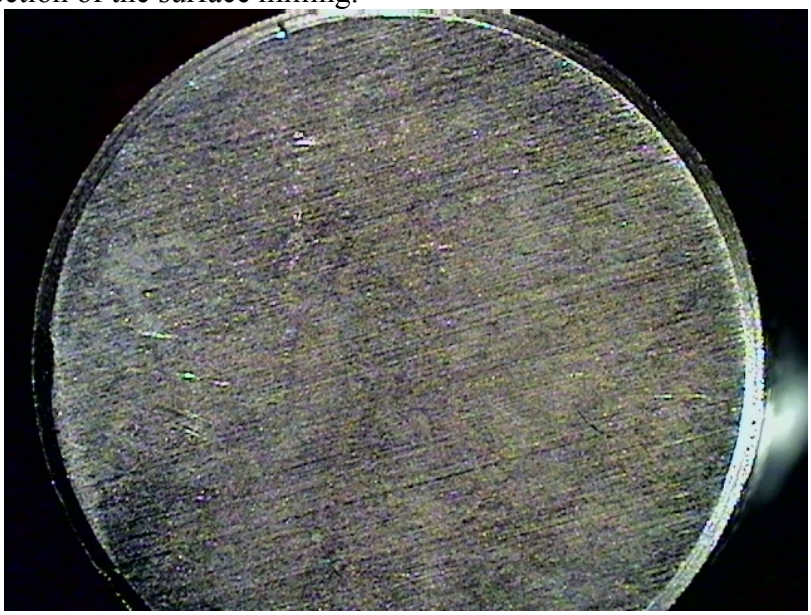

Figure 7. Surface of an as-received A285 sample before testing

Figure 8 shows the results of a typical CPP scan and the analysis of the CPP data using standard corrosion interpretation methods.[12] The specific scan shown in Figure 8 was performed for an A285 coupon at 125°C with concentrations of 12/3/0.2 M (hydroxide/nitrate/nitrite), but the shape of the scan as well as the values for corrosion potential and pitting potential are representative of most other scans. The electrochemical tests performed as part of this study consistently showed electrochemical characteristics indicating that the materials would generally be stable and not be susceptible to SCC.

An example of the positive results shown in Figure 8 is that all of the samples exhibited positive or no hysteresis during CPP experiments. The positive hysteresis indicates the presence of a stable oxide layer on the sample surface. The samples did not exhibit break point potentials that indicate susceptibility to local corrosion. The reversals in the scanning direction were caused by reaching current limits set for the experiments and the scan reversal was usually caused by the onset of the transpassive oxygen evolution reaction. During the CPP experiments, the current for nearly all samples reached a plateau value close to 0 V vs. the Hg/HgO reference electrode. A representative CPP experimental result is shown in

Figure 8. The analysis of the CPP scan according to the methods described in WSRC-STI-2006-00029[13] is shown in the diagram.

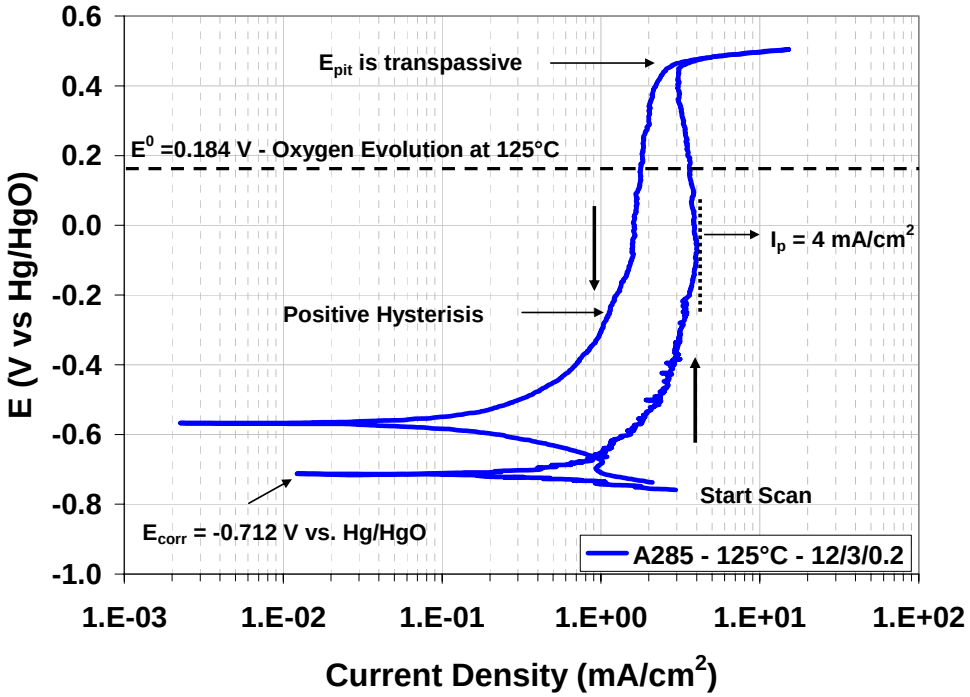

Figure 8. Representative CPP experimental result for an A285 coupon at 125°C in a solution with 12 M hydroxide, 3 M nitrate, and 0.2 M nitrite

Given the generally positive results for unstressed samples, the analysis of the experimental results will focus on understanding differences in the electrochemical behavior of the coupons as reaction conditions are varied. This baseline unstressed electrochemical analysis will assist in the interpretation of data on stressed samples to be collected during phase 2 of this project.

The electrochemical testing of the A285 and A516 coupons included open circuit potential measurements to provide data regarding the stability of the metal in solution, polarization resistance experiments to measure general corrosion rate, and CPP scans to measure localized corrosion susceptibility. The electrochemical experiments were performed while varying the coupon type, the effect of nitrate and nitrite concentration, and dissolved gases, temperature, and hydroxide concentration were investigated. The test conditions together with the corrosion potential, pitting potential, and polarization resistance are shown in Table 1. No discernable trends in the data were seen due to the atmosphere in the tank or the nitrate and nitrite concentrations. The lack of effect from nitrate and nitrite concentrations is similar to conclusions from experiments at lower hydroxide concentrations found in previous studies summarized in WSRC-STI-2006-00029.[13] Therefore, analysis of the data in this report focused on the differences in data due to the material type, hydroxide concentration, and temperature.

Table 1. Experimental conditions and corrosion characteristics extracted from the results

Exp. #	O_2:N_2 Ratio	Material	Temp. (°C)	Hydroxide (M)	Nitrate (M)	Nitrite (M)	E^0 (V vs Hg/HgO)	Epit (V vs Hg/HgO)	Rp (Ohms)
1	0.2 : 0.8	A285	60	6	1	0.2	-0.646	N/A	1750
2	0.2 : 0.8	A516	60	6	1	0.2	-0.377	N/A	2980
3	0.2 : 0.8	A285	60	6	1	1	-0.582	N/A	2170
4	0.2 : 0.8	A516	60	6	1	1	-0.404	N/A	N/A
5	0.2 : 0.8	A285	60	6	3	0.2	-0.537	N/A	2410
6	0.2 : 0.8	A516	60	6	3	0.2	-0.813	N/A	154
7	0.2 : 0.8	A285	60	6	3	1	-0.773	0.545	710
8	0.2 : 0.8	A516	60	6	3	1	-0.772	0.553	458
9	0.2 : 0.8	A285	100	6	1	0.2	-0.55	N/A	N/A
10	0.2 : 0.8	A516	100	6	1	0.2	-0.41	0.57	1345
11	0.2 : 0.8	A285	100	6	1	1	-0.587	N/A	1148
12	0.2 : 0.8	A516	100	6	1	1	-0.589	N/A	253
13	0.2 : 0.8	A285	100	6	3	0.2	-0.514	N/A	1033
14	0.2 : 0.8	A516	100	6	3	0.2	-0.525	0.553	610
15	0.2 : 0.8	A285	100	6	3	1	-0.749	0.488	131
16	0.2 : 0.8	A516	100	6	3	1	-0.759	N/A	134
17	0.2 : 0.8	A285	60	8	1	0.2	-0.805	0.551	344
18	0.2 : 0.8	A516	100	8	1	0.2	-0.781	N/A	103
19	0.2 : 0.8	A285	100	8	1	1	-0.603	N/A	82.6
20	0.2 : 0.8	A516	60	8	1	1	-0.764	N/A	88.8
21	0.2 : 0.8	A285	60	8	3	0.2	-0.775	0.502	355.7
22	0.2 : 0.8	A516	100	8	3	0.2	-0.719	N/A	127
23	0.2 : 0.8	A285	100	8	3	1	-0.668	N/A	101
24	0.2 : 0.8	A516	60	8	3	1	-0.812	N/A	64.5
25	0.2 : 0.8	A285	125	12	1	0.2	-0.706	N/A	60.5
26	0.2 : 0.8	A516	125	12	1	0.2	-0.812	N/A	62.5
27	0.2 : 0.8	A285	125	12	1	1	-0.712	N/A	21.8
28	0.2 : 0.8	A516	125	12	1	1	-0.709	N/A	38.6
29	0.2 : 0.8	A285	125	12	3	0.2	-0.739	0.504	32.7
30	0.2 : 0.8	A516	125	12	3	0.2	-0.767	0.474	N/A
31	0.2 : 0.8	A285	125	12	3	1	-0.729	N/A	6.78
32	0.2 : 0.8	A516	125	12	3	1	-0.67	0.494	27.2
33	0.5 : 0.5	A285	60	6	1	0.2	-0.767	0.58	663
34	0.5 : 0.5	A516	60	6	1	1	-0.503	0.522	1921
35	0.5 : 0.5	A285	60	6	3	0.2	-0.404	0.607	1384
36	0.5 : 0.5	A516	60	6	3	1	-0.44	0.547	1114
37	0.5 : 0.5	A285	100	6	3	0.2	-0.78	0.543	390
38	0.5 : 0.5	A516	100	6	3	1	-0.691	0.468	176
39	0.5 : 0.5	A285	125	12	1	1			
40	0.5 : 0.5	A516	125	12	3	1			
41	0.0 : 1.0	A285	60	6	1	0.2	-0.308	0.567	2638
42	0.0 : 1.0	A516	60	6	1	1	-0.752	0.587	925
43	0.0 : 1.0	A285	60	6	3	0.2	-0.409	0.509	3124
44	0.0 : 1.0	A516	60	6	3	1	-0.752	0.533	214
45	0.0 : 1.0	A285	100	6	3	0.2	-0.738	N/A	380
46	0.0 : 1.0	A516	100	6	3	1	-0.758	N/A	82
47	0.0 : 1.0	A285	125	12	1	1	-0.715	N/A	27.7
48	0.0 : 1.0	A516	125	12	3	1	-0.725	N/A	N/A

The pitting potentials measured in the scans were between 468 and 607 mV above the potential of the Hg/HgO reference electrode and these values are all well above equilibrium potential for the oxygen evolution reaction. Therefore, the large currents above the pitting potential are likely caused by oxygen evolution in the transpassive region.

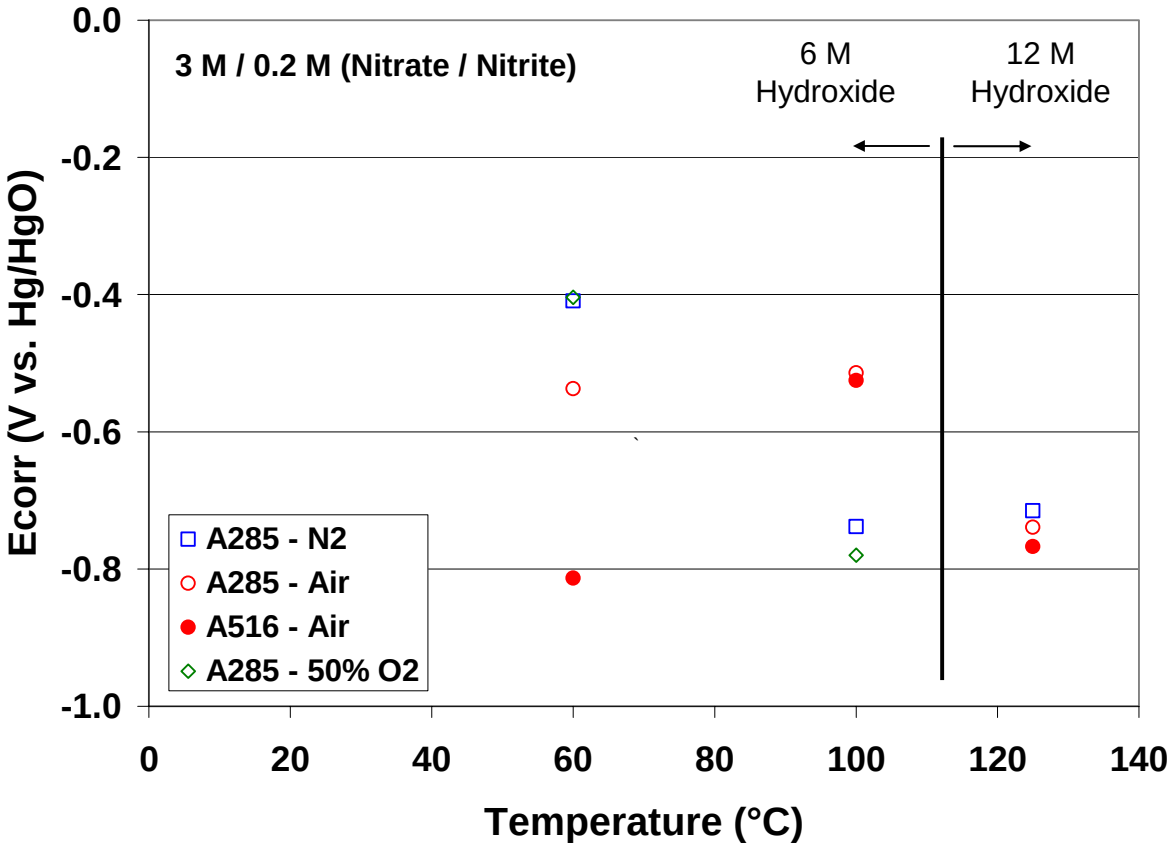

Figure 9. Corrosion potentials for experiments with 3 M / 0.2 M (Nitrate/Nitrite) concentrations

Figure 9 shows the effect of temperature on the corrosion potential for samples in a solution with 3 M nitrate and 0.2 M nitrite concentrations. The open points in Figure 9 represent the corrosion potential data for A285 samples and the solid points represent data for A516 samples. The shape of the data points represents the dissolved gas with squares for nitrogen, circles for air, and diamonds for a 50:50% O_2/N_2 gas mixture. Tests were performed with 6 M hydroxide concentrations at 60°C and 100°C while tests at 125°C were performed with a 12 M hydroxide concentration. The data in this figure show significant scatter with dissolved gas and steel type. The scatter in the data is larger at lower temperatures than at higher temperatures. As mentioned in the review of literature, researchers working with similar systems[14] saw reduced reproducibility at lower temperatures and that was attributed to initial state of the sample surfaces and slower kinetics at low temperature. At 100°C and 125°C, the corrosion potential ranges were reduced from 60°C experiments and were more uniform. The reduced corrosion potentials for the higher temperatures are predicted by thermodynamic calculations that are described below and the increased corrosion potential uniformity is

likely due to the faster reaction kinetics that bring the react the as-received surface to a relatively uniform state quickly.

The electrochemical potentials under the conditions in this study were calculated using a commercial thermodynamics software package (HSC Chemistry, Outokumpu) and are shown in Table 2, below. The thermodynamic calculations predict that the equilibrium potentials decrease with increasing temperature and hydroxide concentration. These trends are seen in the overall data set where the maximum corrosion potential decreases with increasing temperature and hydroxide concentration.

The electrochemical equilibrium potential data delineates whether specific reactions are possible at a given potential and which reactions are thermodynamically preferred. For example, while performing an oxidation on an iron electrode surface at 60°C, the oxidation of metallic iron to iron (II) hydroxide, $Fe(OH)_2$, can occur at potentials above -1.061 V versus an Hg/HgO reference electrode. Also, the oxidation of metallic iron to Fe_3O_4 only occurs above -0.971 V vs. Hg/HgO. Therefore, if the potential is above -1.061 V, but below -0.971, then the oxidation of iron to $Fe(OH)_2$ is possible, but its oxidation to Fe_3O_4 is not. This analysis can help researchers understand what is happening on the sample surface at different potentials.

In the experiments detailed in this report, the corrosion potentials are above -0.815 V vs. Hg/HgO. Therefore, the metallic iron on the surface has already been oxidized to form surface oxides such as $Fe(OH)_2$, FeOOH, and Fe_3O_4. Corrosion potentials in the range of -0.815 to -0.377 V indicate equilibrium between the different surface oxides and that changes in the corrosion potential reflect alteration in the oxide layer structure. The potentials where sustained electrochemical reactions occur can be relatively far away from the equilibrium potential values due to the overpotential needed to drive specific reactions. Therefore, the table of reduction potentials should be mainly used for analyzing equilibrium data and understanding possible reactions at different potentials.

Table 2. Iron electrode reactions and equilibrium potentials under experimental conditions

Electrode Reaction	E^0 (V vs. Hg/HgO) @ 60°C			E^0 (V vs. Hg/HgO) @ 100°C			E^0 (V vs. Hg/HgO) @ 125°C
	$[OH]^-$= 6 M	$[OH]^-$= 8 M	$[OH]^-$= 12 M	$[OH]^-$= 6 M	$[OH]^-$= 8 M	$[OH]^-$= 12 M	$[OH]^-$= 12 M
$O_2 + 2H_2O + 4e^- \leftrightarrow 4OH^-$	0.238	0.231	0.220	0.216	0.209	0.198	0.184
$FeO_2^- + 2H_2O + e^- \leftrightarrow Fe_3O_4 + 4OH^-$	-0.108	-0.115	-0.126	-0.140	-0.147	-0.158	-0.171
$3Fe(OH)_3 + e^- \leftrightarrow Fe_3O_4 + 4H_2O + OH^-$	-0.150	-0.157	-0.168	-0.081	-0.088	-0.099	-0.053
$FeOOH + e^- \leftrightarrow Fe_3O_4 + H_2O + OH^-$	-0.720	-0.727	-0.738	-0.689	-0.696	-0.707	-0.686
$3Fe_2O_3 + H_2O + 2e^- \leftrightarrow 2Fe_3O_4 + 2OH^-$	-0.737	-0.787	-0.798	-0.732	-0.739	-0.750	-0.745
$Fe(OH)_3 + e^- \leftrightarrow Fe(OH)_2 + 3OH^-$	-0.761	-0.768	-0.779	-0.751	-0.758	-0.769	-0.762
$FeO_2^- + 2H_2O + e^- \leftrightarrow Fe(OH)_2 + 2OH^-$	-0.747	-0.754	-0.765	-0.770	-0.777	-0.788	-0.801
$Fe(OH)_3 + 3e^- \leftrightarrow HFeO_2^- + H_2O$	-0.870	-0.870	-0.870	-0.880	-0.880	-0.880	-0.882
$HFeO_2^- + H_2O + 2e^- \leftrightarrow Fe + 3OH^-$	-0.892	-0.885	-0.874	-0.882	-0.877	-0.864	-0.858
$FeO_2^- + H_2O + e^- \leftrightarrow HFeO_2^- + OH^-$	-0.902	-0.909	-0.920	-0.945	-0.952	-0.963	-0.985
$FeOOH + H_2O + e^- \leftrightarrow Fe(OH)_2 + OH^-$	-0.951	-0.958	-0.969	-0.954	-0.961	-0.972	-0.973
$Fe_3O_4 + 4H_2O + 8e^- \leftrightarrow 3Fe + 8OH^-$	-0.971	-0.964	-0.953	-0.975	-0.968	-0.957	-0.960
$FeO_2^- + 2H_2O + 3e^- \leftrightarrow Fe + 4OH^-$	-0.957	-0.964	-0.975	-0.964	-0.971	-0.982	-0.986
$Fe_2O_3 + 3H_2O + 2e^- \leftrightarrow Fe(OH)_2 + 2OH^-$	-0.957	-0.964	-0.975	-0.968	-0.975	-0.986	-0.993
$Fe(OH)_3 + 3e^- \leftrightarrow Fe + 3OH^-$	-0.961	-0.968	-1.079	-0.958	-0.965	-0.848	-0.973
$2H_2O + 2e^- \leftrightarrow H_2 + 2OH^-$	-0.962	-0.969	-0.980	-0.952	-0.959	-0.970	-0.963
$FeOOH + H_2O + 3e^- \leftrightarrow Fe + 3OH^-$	-1.025	-1.032	-1.043	-1.025	-1.032	-1.043	-1.043
$Fe_2O_3 + 3H_2O + 6e^- \leftrightarrow 2Fe + 6OH^-$	-1.026	-1.033	-1.044	-1.030	-1.037	-1.048	-1.050
$Fe(OH)_2 + 2e^- \leftrightarrow Fe + 2OH^-$	-1.061	-1.068	-1.079	-1.061	-1.068	-0.951	-1.078
$Fe_3O_4 + 4H_2O + 2e^- \leftrightarrow 3Fe(OH)_2 + 2OH^-$	-1.066	-1.073	-1.084	-1.086	-1.093	-1.104	-1.117
$Fe_3O_4 + H_2O + OH^- + 2e^- \leftrightarrow 3HFeO_2^-$	-1.298	-1.305	-1.316	-1.348	-1.355	-1.366	-1.393

Figure 10 shows the effect of temperature on the corrosion potential for samples in a solution with 3 M nitrate and 1 M nitrite concentrations. The open points in Figure 10 represent the corrosion potential data for A516 samples and the solid points represent data for A285 samples. The shape of the data points represents the dissolved gas with squares for nitrogen, circles for air, and diamonds for a 50:50% O_2/N_2 gas mixture. Tests were performed with 6 M hydroxide concentrations at 60°C and 100°C while tests at 125°C were performed with a 12 M hydroxide concentration. This is likely a similar effect to the high scatter seen at low temperatures in Figure 9. The data in this graph are more closely grouped at each temperature with the exception of the experiments with a 50% O_2 /50% N_2 dissolved gas mixture that had more noble corrosion potentials. However, the high potentials for the 50% O_2 /50% N_2 dissolved gas mixture were not seen in data sets for other conditions. The corrosion potential data in Figure 10 appear to stay relatively constant with increasing temperature.

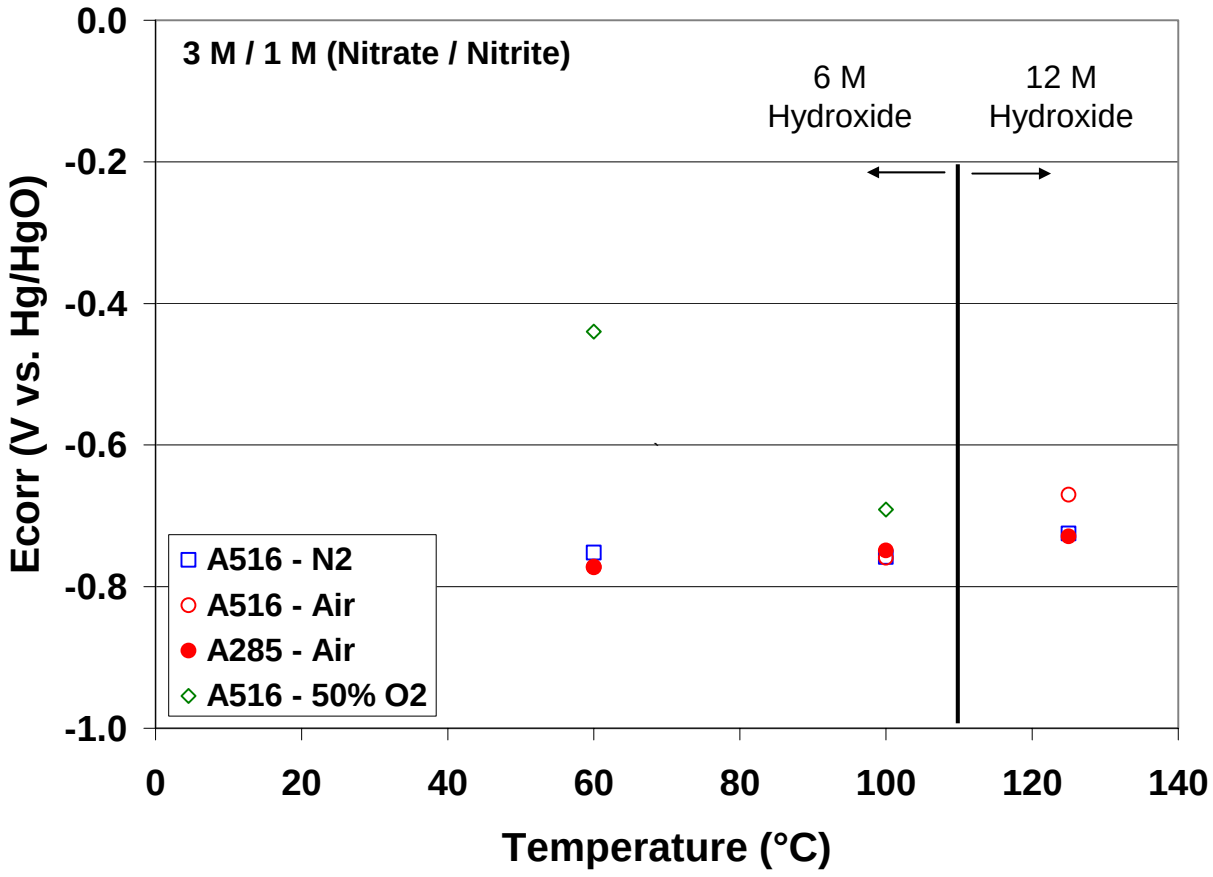

Figure 10. Corrosion potentials for experiments with 3 M / 1 M (Nitrate/Nitrite) concentrations

Figure 11 shows the entire data set for corrosion potential in atmospheres with varying oxygen content at different temperatures. The other experimental variables (nitrate concentration, nitrite concentration, hydroxide concentration, and temperature) in Figure 11 are not held constant. There is no discernable effect of the vessel atmosphere on the corrosion potential measured during the electrochemical experiments. Additionally, the

concentration of nitrate and nitrite in the solutions did not have a significant effect on the corrosion potential. Therefore, the data at each temperature was grouped and averaged for each type of steel at each temperature when analyzing the passivation current and polarization in the following figures.

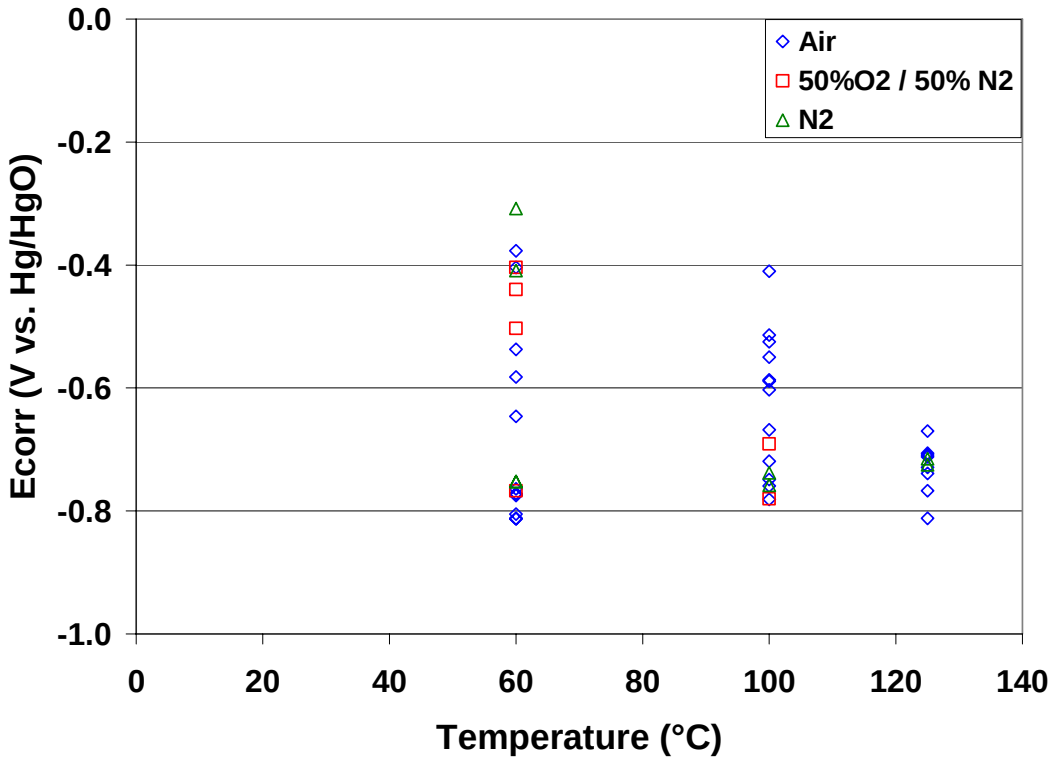

Figure 11. Corrosion potential for experiments performed in different atmospheres and at different temperatures.

Figure 12 shows the current density values for the reaction occurring in this potential range for A285 and A516 samples at different experimental temperatures. The current at the electrodes increased exponentially as temperature increased. The current densities for the A516 electrodes had a slightly higher median value than the currents for the A285 electrodes at 60°C and 100°C, but nearly the same value at 125°C. At the lower temperatures, there was larger scatter in the current data that is most likely due to surface variations in the as received samples. When the temperature increased, the scatter in the data was reduced and the results from the A285 and A516 samples converged to nearly the same value.

The current results in Figure 12 are centered on 1 mA/cm^2 and the samples usually showed a sustained current near this value during the 4 hour scan. Literature data from the constant current oxidation of iron electrodes in caustic solutions has shown that oxidation under these current conditions can take place for over 6 hours at 25°C [8] and that the time the electrode can sustain an oxidation current without changing potential increases with reaction temperature.[5, 7] Therefore, the current behavior that was observed in the designed experimental plan is representative of alloy surfaces that are freshly exposed to caustic solutions. The behavior of the alloy surfaces during prolonged exposure to caustic solutions

should also be characterized to understand the evolution of the passive layer on the alloy surfaces with time. Additionally, long-term studies of the alloy surface electrochemistry may provide insight about the feasibility of protecting the surface through anodic protection methods.

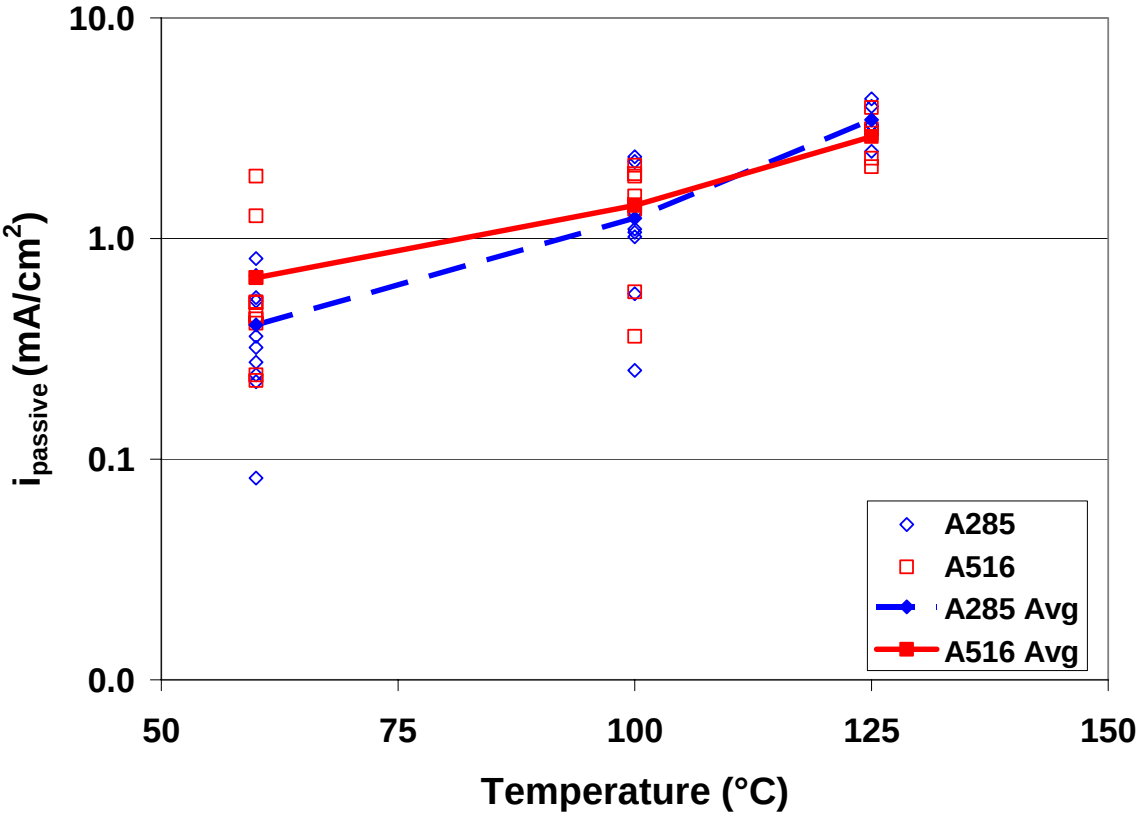

Figure 12. Passive current densities for A285 and A516 coupons during CPP scans at different temperatures

The polarization resistance of the samples was regressed from a small amplitude cyclic voltammetry experiment around the corrosion potential of the samples at a scan rate of 0.17 mV/s. The polarization resistance is inversely proportional to the corrosion rate of the samples. In other words, a sample with a high polarization resistance will have a low corrosion rate while a sample with a low polarization resistance will have a high corrosion rate. Figure 13 shows the polarization resistance of the A285 and A516 carbon steel coupons at 60°C, 100°C, and 125°C. The polarization resistance decreased as the temperature of the solution increased, thus indicating an increased rate of corrosion. The decrease in the average polarization resistances for both the A285 and A516 samples over a 55°C increase in temperature was around 55 times and 40 times, respectively. Additionally, most of the decrease in the polarization resistance occurred between 100°C and 125°C.

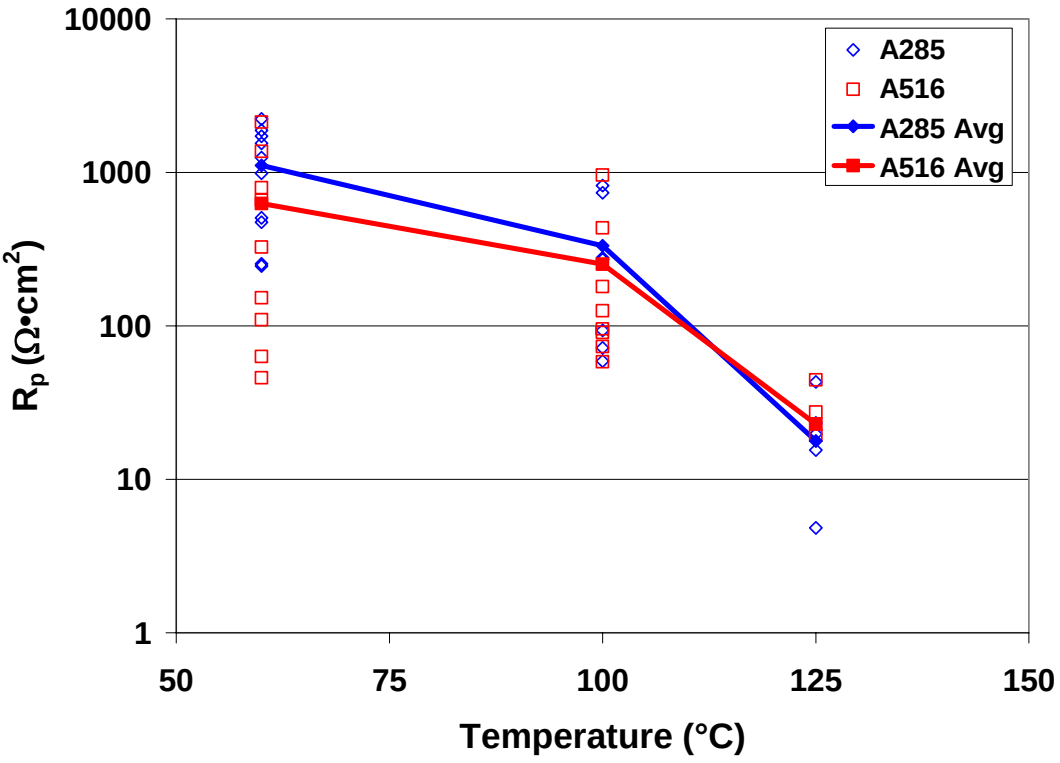

Figure 13. Polarization resistance for A285 and A516 samples at different temperatures

The polarization resistances shown in Figure 13 were used to estimate the corrosion rate of the samples using the equation:

$$r_{corr}[mpy] = 456 \bullet \frac{B}{R_p}$$

Where r_{corr} is the corrosion rate in mils per year (mpy), B is the effective tafel slope in mV/decade, and R_p is the polarization resistance in Ω•cm^2. The effective Tafel slope was estimated to be 25 mV/decade for calculation of the corrosion rates. The corrosion rates for all samples at a given temperature have been averaged to calculate theses values. The corrosion rate increases by a factor of 5 over a 25°C increase in temperature from 100°C to 125°C. The sudden increase in corrosion rate reflects the drop in the polarization resistance seen in Figure 13. The 473 mpy average corrosion rate at 125°C is very large and likely indicates a bulk reaction at the surface with no passive film formation.

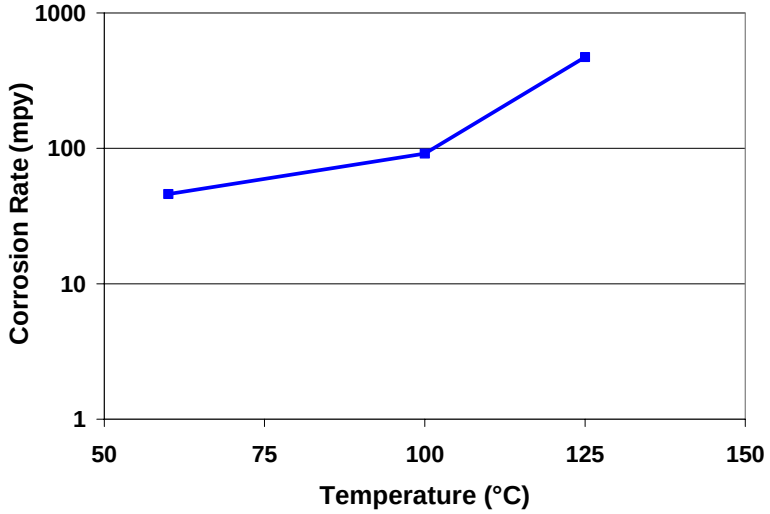

Figure 14. Corrosion rates estimated from polarization resistances. The value at each is averaged over all samples at each solution temperature

A possible explanation for this behavior is that iron oxides are not stable on the surface with the 12 M hydroxide concentration used for experiments at 125°C. At a concentration of 12 M, the pH of the test solution will be near 15.1. The Pourbaix diagram for iron at 125°C is shown in Figure 15 and indicates that near this pH, Fe_3O_4 is not stable in solution and will start to dissolve to form $HFeO_2^-$ and FeO_2^- ions. The dissolution of the iron oxide passive layer on the surface at this high pH would leave the bulk iron atoms in the sample unprotected from dissolution into the solution. This type of reaction mechanism could easily explain the observed behavior.

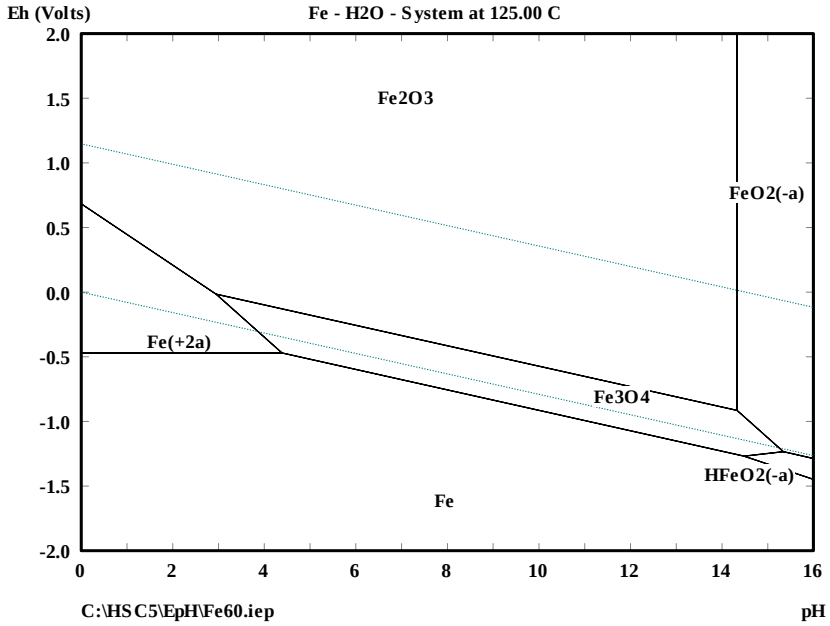

Figure 15. Pourbaix diagram for iron at 125°C

Although the difference between the alloys relative to the data scatter is not large enough to conclusively say that there is a significant difference between the metals, the A516 carbon steel contains more elements such as Mn, Ni, and Cu that should be more stable in this high pH range. The chemical compositions for A285 and A516 steels are given in Table 3. If iron is being removed from the surface at high hydroxide concentrations, the surface of the metal should have higher proportions of the compounds that are stable at high pH. To confirm the importance of these elements in providing corrosion resistance, surface studies using XRD, EDX, and XPS could be performed on samples exposed for long times to the high pH.

Table 3. Composition of A285 and A516 carbon steels. [15]

Table 1. Chemical composition of A 285 and A 516 steels (wt %).

Steel	*C*	*Mn*	*P*	*S*	*Si*	*Cu*	*Ni*	*Cr*	*Mo*	*Sr*	*Fe*
A 285	0.19	0.71	0.020	0.016	0.01	0.007	0.004	0.033	0.004	0.002	balance
A 516	0.24	1.15	0.008	0.007	0.25	0.044	0.025	0.033	0.004	0.002	balance

4.2 COMPARISONS WITH PREVIOUS TESTING

The experimental results from testing detailed in this report were compared with the previous electrochemical results reported in WSRC-TR-2004-00292,[16] SRT-MTS-984159,[17] WSRC-TR-2003-00370,[18] SRNS-STI-2009-00564,[19] and literature data[15]. A couple of significant differences between the current results and previous tests are: 1) the lack of an active-passive transition that suggests localized corrosion susceptibility, and 2) significantly higher corrosion rates than long term tests. The differences in the current and previous data indicate effects caused by corrosion inhibitors and a large decrease in the corrosion rate over time.

Testing results in WSRC-TR-2004-00292 concluded that carbon steels in solutions with a hydroxide concentration of 10 M and a nitrate concentration of 2 M showed an active-passive transition in anodic polarization experiments that indicates susceptibility to localized corrosion. Additionally, the testing in WSRC-TR-2004-00292 showed higher localized corrosion susceptibility in solution without dissolved oxygen. However, the test solutions in those experiments did not contain nitrite. The lack of an strong oxidizing agent in solution may have decreased repassivation of defects in the metal surface and thus led to the active-passive transition.

The testing results in this report contain nitrite ions and it the differences in the results suggest that at high temperatures nitrite ions play an important role in protecting the tank surface. To look at the effect of inhibitors on caustic corrosion of carbon steels. To analyze the effects of inhibitors, a ratio of hydroxide ions to inhibitor ions has been defined as:

$$R = \frac{[OH^-]}{[NO_3^-]+[NO_2^-]}$$

Figure 16 shows the R value and temperature at which experiments were performed in this study, WSRC-TR-2004-00292, and SRNS-STI-2009-00564. The shape and color of the data points indicate the reference and also whether the data showed an active passive transition

that may indicate localized corrosion. In general, the studies performed with an R value less than 10 showed no susceptibility to SCC while all experiments with R values greater than 10 exhibited localized corrosion. The exceptions to this analysis were two experiments at 95°C from WSRC-TR-2004-00292. At temperatures of 95°C and higher, the only samples that did not experience localized corrosion were tested in solutions that contained nitrite ions. Nitrite ions are strong oxidizing agents and may more aggressively help to passivate the tank surface at high temperatures. The lowest nitrite concentration tested was 0.2 M. Further experiments could be designed to test the effectiveness of nitrites to prevent localized corrosion under high temperature high hydroxide concentrations.

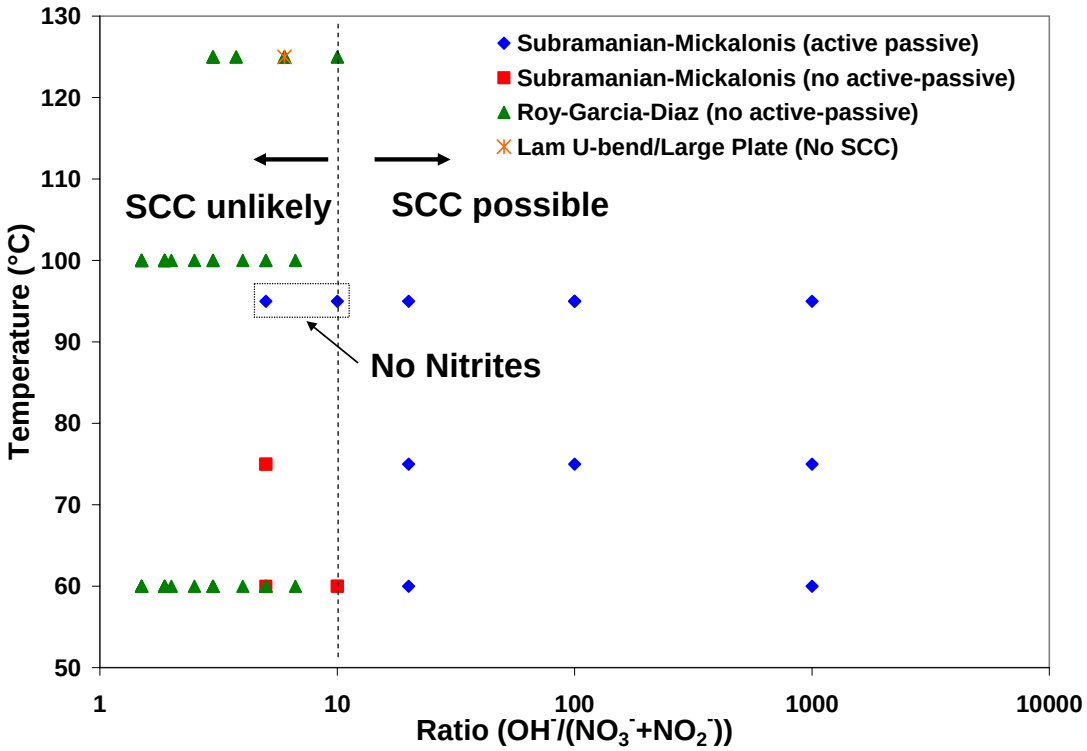

Figure 16. Corrosion results for experiments with varying hydroxide to inhibitor ratio and varying temperature.

Another interesting between the results in this report and previous testing are the high corrosion rates measured in polarization resistance experiments. The average of the corrosion rates shown in Figure 14 are between 40 and 400 mpy. However, tests on U-bend samples, large steel plates, and service histories of the waste tanks generally measure corrosion rates less than 1 mpy.[17-19] The difference of more than an order of magnitude between the long-term corrosion rate and the value measured from the polarization resistance could be explained by a significant decrease in the corrosion rate after a brief reaction period at the start of testing. In the current testing, samples were equilibrated in the test solution at room temperature for one day before testing and at the test temperature for an hour before testing. Results from Le and Ghali[15] showed that the corrosion potential for A285 and A516 coupons in solution with 7 M of hydroxide increased significantly between 3 and 30 hours. Figure 17 [15] shows the increase in the corrosion potential at room temperature. The jump in the corrosion potential is very rapid and is similar to the jumps in potential seen in constant

current experiments as shown in Figure 1 and Figure 6. Therefore, the potential increase is likely due to a change in the surface oxide on the samples. The corrosion potentials from current testing that summarized in Table 1 are in the range of the first plateaus of Figure 17.

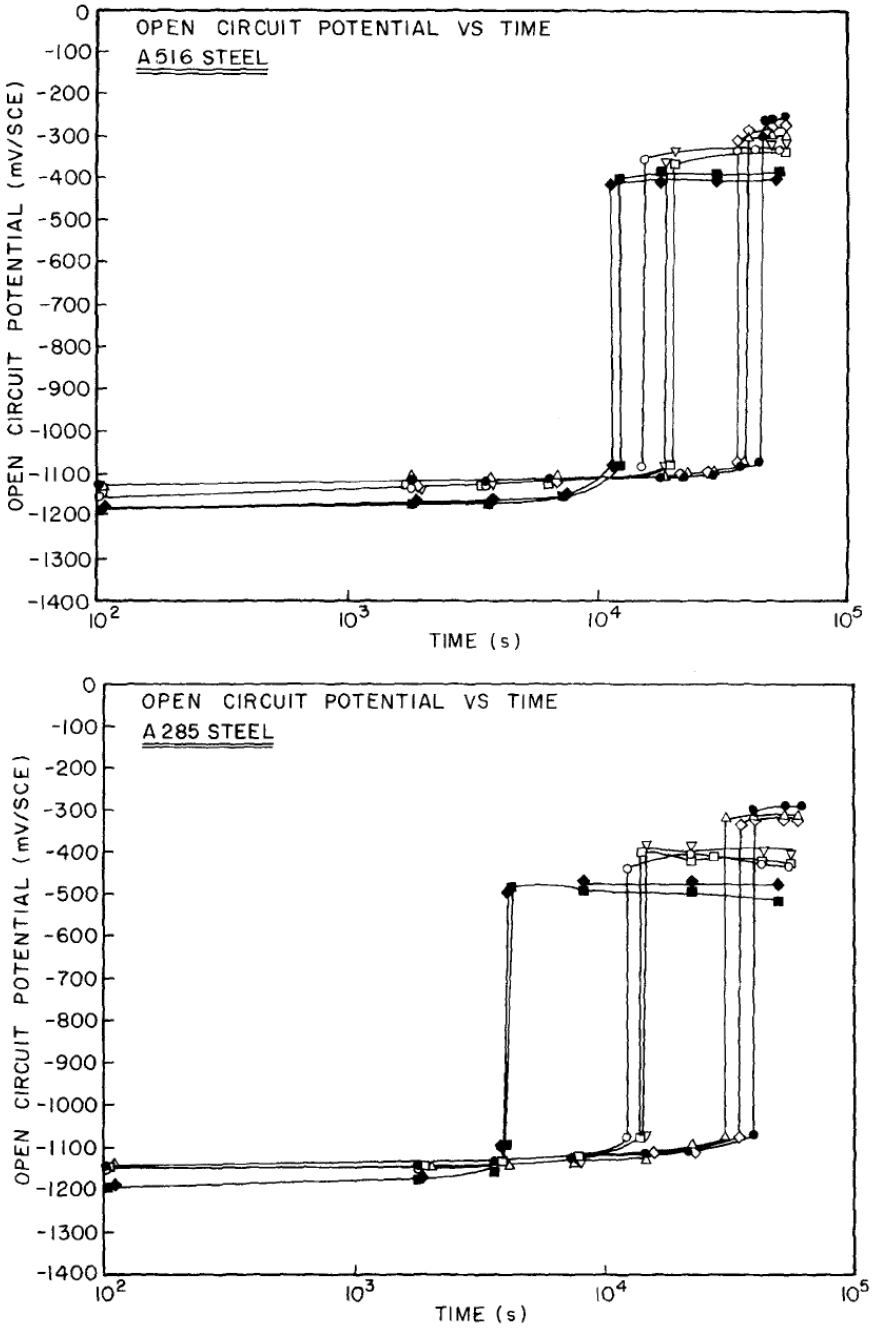

Figure 17. Extended corrosion potential for A516 and A285 steels at room temperature

It is suggested that additional experiments are performed to examine the evolution of the corrosion potential at the reaction temperatures with time to ensure that CPP testing is performed when the surface oxide species have adopted their long-term chemistry. Surface

science studies on the samples before and after a transition in potential would provide insight about differences in the surface transition with time.

5.0 PATH FORWARD

5.1 PHASE II TESTING:

The data generated from the Phase I testing will be utilized in future testing during the second phase of this investigation. The second phase of this investigation will involve metallurgical characterization and mechanical testing to determine the susceptibility of steels to stress corrosion cracking (SCC). The susceptibility to SCC will be determined using both slow strain rate and fracture mechanisms based double cantilever beam (DCB) testing techniques. Further, the fractography of the tested specimens will be evaluated by scanning electron microscopy (SEM). Upon completion of testing, the resultant data will be utilized to establish the long-term chemistry and temperature requirements, and their ranges to alleviate SCC susceptibility, and provide input to the technical justification of the corrosion control program.

5.1.1 Tensile Testing

The ambient-temperature tensile properties of both materials will be determined by using smooth cylindrical specimens according to the ASTM Designation E 8. A gauge length to gauge diameter ratio of 4.0 will be maintained for all specimens. The magnitude of yield strength (YS), ultimate tensile strength (UTS), percent elongation (%El) and percent reduction of area (%ROA) will be determined from duplicate testing.

5.1.2 SCC Testing – Constant Displacement Method

SCC testing using wedge-loaded and pre-cracked rectangular double-cantilever-beam (DCB) specimens is currently well accepted to the scientific community. A basic advantage to this method is the simplicity in testing since it does not need any load control. Double-taper wedges of different thicknesses will be inserted into the specimen slot, thus keeping the displacement between the two arms fixed. The cracking susceptibility of carbon steels in similar environments (Table 4 in Appendix A) using this technique will be evaluated in terms of stress intensity factor (K) corresponding to the different levels of load imparted by the wedges of different thicknesses, and the changes in crack length.

5.1.3 SCC Testing – Slow Strain Rate Method

The SCC behavior of both carbon steels will also be evaluated using smooth cylindrical specimens loaded in tension under a slow strain rate of 3.3×10^{-6} sec^{-1} in the presence of similar aqueous environments (Table 4 in Appendix A). The application of this slow strain rate (SSR) will enable the test specimens to undergo failure due to the synergistic effect of applied load and environmental species. The cracking tendency will be characterized by %El, %RA, time-to-failure (TTF), and true failure stress (σ_f). The magnitude of σ_f will be based on the failure load under a specific environmental condition, and the final cross sectional area of the gage section at failure. Cracking tendency under anodic or cathodic applied potential may also be performed under SSR conditions.

5.1.4 Fractographic Evaluations

The extent and morphology of failures of the specimens to be used in SCC testing will be analyzed by scanning electron microscopy (SEM). SCC failures could be either ductile or brittle depending on the test material and environment. Ductile failures are characterized by dimples. On the other hand, brittle failures can be classified into cleavage and intergranular cracking. A combination of transgranular and intergranular cracking may also be seen in some tested specimens. Intergranular corrosion may also be observed on the surfaces of the polarized specimens.

Both the primary and secondary cracks in the SSR specimens will be analyzed by SEM and optical microscopy. A distribution of secondary cracks along the gage section of the tested cylindrical specimens will be developed from the polished metallographic mounts.

Energy dispersive spectrometry (EDS) will be used to analyze the presence and concentration of chemical species in the vicinity of the cracked region. The resultant spectra will enable the determination of the causes of failures of the tested materials, leading to a mechanistic understanding of SCC.

5.2 FUTURE SUGGESTED WORK

5.2.1 Cyclic Voltammetry Studies

Previous cyclic voltammetry studies [6, 10] showed a change in the shape of cyclic voltammograms at the same temperature where SCC starts to be observed in carbon steels. Detailed CV studies have not been performed on A285 and A516 carbon steels to investigate this change in mechanism. In addition, the effects of additives in the electrolyte have also not been investigated.

The proposed study would perform CV scans of both A285 and A516 at temperatures between room temperature and 125°C. The samples would be increased in temperature and CVs would be collected every 10°C. The development of peaks in the CV spectrum with temperature will provide information on reaction mechanisms with temperature. The effect of solution concentrations on the reaction mechanism can also be studied by repeating these studies in solutions with varying solution concentration. Studies where the CV scan is reversed at different potentials will be performed at key temperatures to correlate the oxidation and reduction peaks during the scan.

5.2.2 Constant Current Oxidation Studies

Constant current oxidation experiments were used by researchers investigating iron oxidation to characterize changes in the surface species on an iron electrode.[4, 5, 7] Researchers have also observed large and rapid changes the open circuit on A285 and A516 electrode that are exposed to hydroxide solution for long times.[15] It is proposed to collect longer-term corrosion potentials over 1-2 weeks at different solution temperatures. Aged samples will then be oxidized at constant current and studied using SEM and XRD to characterize surface species. The surface of these samples will be compared with the surface of the Type IV tanks.

After aging of coupons for long times, the samples will also be tested using the CPP technique. The differences between the CPP results from fresh samples and aged samples will be used to understand the changes in SCC susceptibility as tanks age.

6.0 CONCLUSIONS

Electrochemical testing was performed on A285 and A516 coupons to investigate difference in the corrosion of the carbon steels. The testing simulated changes in the solution chemistry, atmosphere, and temperature that occur in Type IV waste tanks at the Savannah River Site that contain concentrated waste from the PUREX process. The experiments performed in this study are the first phase of a two phase study to determine the susceptibility of Type IV waste tanks to Stress Corrosion Cracking (SCC). Phase I testing consisted of electrochemical testing of unstressed coupons in a simulated tank environment.

Electrochemical testing included measurement of the corrosion potential and polarization resistance as well as Cyclic Potential Polarization (CPP) testing of coupons. CPP results showed no indications of localized corrosion such as pitting and all samples showed the formation of a stable passive layer as evidenced by the positive hysteresis during the scan. Analysis of the CPP data was performed to compare the corrosion susceptibility of the samples under different environmental conditions.

Testing revealed that the most important factors affecting the corrosion of the tanks are the solution temperature, solution pH, and the material used in constructing the tank. Variables that did not significantly affect the corrosion susceptibility of the tanks were the nitrate or nitrite concentration and the atmosphere in the tank. The passivation current for the coupons increased exponentially with temperature. Longer term studies of the passivation current are suggested based on literature data for iron in highly caustic environments. Polarization resistance studies showed a dramatic increase in corrosion susceptibility at test conditions of 125°C and 12 M hydroxide concentration. In the temperature and pH range of these tests, iron oxide, Fe_3O_4, becomes unstable and could account for the increased corrosion susceptibility. The applicability of these conditions should be confirmed and detailed surface studies should be conducted to determine the corrosion resistance of A285 and A516 carbon steels under these conditions. Surface science studies should also be conducted to determine the role of the carbon steel chemistry in preventing corrosion under these conditions.

7.0 REFERENCES

1. B. J. Wiersma, *An Assessment of the Service History and Corrosion Susceptibility of Type IV Waste Tanks*, SRNS-STI-2008-00096, C-ESR-G-00007, 2008.
2. R. S. Ondrejcin, *Prediction of Stress Corrosion of Carbon Steel by Nuclear Process Liquid Wastes*, DP-1478, 1978.
3. R. K. S. Raman and A. Saxena, Journal of the Electrochemical Society, 2007. **154**(9): p. C451-C457.
4. A. J. Salkind, C. J. Venuto, and S. U. Falk, Journal of the Electrochemical Society, 1964. **111**(5): p. 493-495.
5. B. Andersson and L. Ojefors, Journal of the Electrochemical Society, 1976. **123**(6): p. 824-828.
6. Macdonal.Dd and D. Owen, Journal of the Electrochemical Society, 1973. **120**(3): p. 317-324.
7. L. Ojefors, Journal of the Electrochemical Society, 1976. **123**(11): p. 1691-1696.
8. H. G. Silver and E. Lekas, Journal of the Electrochemical Society, 1970. **117**(1): p. 5-&.
9. H. Y. Zhang and S. M. Park, Journal of the Electrochemical Society, 1994. **141**(3): p. 718-724.
10. A. Wieckowski, E. Ghali, and H. H. Le, Journal of the Electrochemical Society, 1984. **131**(9): p. 2024-2027.
11. A. K. Roy, M. K. Spragge, D. L. Fleming, and B. Y. Lum, Micron, 2001. **32**(2): p. 211-218.
12. B. J. Wiersma, *Task Plan for the Determination of Corrosion Inhibitor Criteria for Type III/IIIA Tanks During Salt Dissolution Operations*, SRNL-MTS-2005-50019, 2005.
13. B. J. Wiersma and J. I. Mickalonis, *Determination of Corrosion Inhibitor Criteria for Type III/IIIA Tanks During Salt Dissolution Operations (U)*, WSRC-STI-2006-00029, 2006.
14. D. Macdonald and D. Owen, Journal of the Electrochemical Society, 1973. **120**(3): p. 317-324.
15. H. H. Le and E. Ghali, Journal of Applied Electrochemistry, 1992. **22**(4): p. 396-403.
16. K. H. Subramanian and J. I. Mickalonis, *Anodic Polarization Behavior of Low-Carbon Steel in Concentrated Sodium Hydroxide and Sodium Nitrate Additions*, WSRC-TR-2004-00292, 2004.
17. C. F. Jenkins, *Caustic Corrosion of Carbon Steel - Applications to RHLWE Runs*, SRT-MTS-984159, 1998.
18. J.B. Elder, *Tank Inspection NDE Results for Fiscal Year 2003 Including HLW Tanks 30, 31, 32, and 34*, WSRC-TR-2003-00370, 2003.
19. P. S. Lam, *Investigation of the Potential for Caustic Stress Corrosion Cracking of A537 Carbon Steel Nuclear Waste Tanks*, SRNS-STI-2009-00564, 2009.

8.0 APPENDIX A

Table 4. Test Matrix for Electrochemical Testing

Experiment #	O_2:N_2 Ratio	Material	Hydroxide (M)	Nitrate (M)	Nitrite (M)	Temperature (°C)
1	0.2:0.8	A285	6	1	0.2	60
2	0.2:0.8	A516	6	1	0.2	60
3	0.2:0.8	A285	6	1	1	60
4	0.2:0.8	A516	6	1	1	60
5	0.2:0.8	A285	6	3	0.2	60
6	0.2:0.8	A516	6	3	0.2	60
7	0.2:0.8	A285	6	3	1	60
8	0.2:0.8	A516	6	3	1	60
9	0.2:0.8	A285	6	1	0.2	100
10	0.2:0.8	A516	6	1	0.2	100
11	0.2:0.8	A285	6	1	1	100
12	0.2:0.8	A516	6	1	1	100
13	0.2:0.8	A285	6	3	0.2	100
14	0.2:0.8	A516	6	3	0.2	100
15	0.2:0.8	A285	6	3	1	100
16	0.2:0.8	A516	6	3	1	100
17	0.2:0.8	A285	8	1	0.2	60
18	0.2:0.8	A516	8	1	0.2	100
19	0.2:0.8	A285	8	1	1	100
20	0.2:0.8	A516	8	1	1	60
21	0.2:0.8	A285	8	3	0.2	60
22	0.2:0.8	A516	8	3	0.2	100
23	0.2:0.8	A285	8	3	1	100
24	0.2:0.8	A516	8	3	1	60
25	0.2:0.8	A285	12	1	0.2	125
26	0.2:0.8	A516	12	1	0.2	125
27	0.2:0.8	A285	12	1	1	125
28	0.2:0.8	A516	12	1	1	125
29	0.2:0.8	A285	12	3	0.2	125
30	0.2:0.8	A516	12	3	0.2	125
31	0.2:0.8	A285	12	3	1	125
32	0.2:0.8	A516	12	3	1	125
33	0.5:0.5	A285	6	1	0.2	60
34	0.5:0.5	A516	6	1	1	60
35	0.5:0.5	A285	6	3	0.2	60
36	0.5:0.5	A516	6	3	1	60
37	0.5:0.5	A285	6	3	0.2	100
38	0.5:0.5	A516	6	3	1	100
39	0.5:0.5	A285	12	1	1	125
40	0.5:0.5	A516	12	3	1	125
41	0.0:1.0	A285	6	1	0.2	60
42	0.0:1.0	A516	6	1	1	60
43	0.0:1.0	A285	6	3	0.2	60
44	0.0:1.0	A516	6	3	1	60
45	0.0:1.0	A285	6	3	0.2	100
46	0.0:1.0	A516	6	3	1	100
47	0.0:1.0	A285	12	1	1	125
48	0.0:1.0	A516	12	3	1	125

Table 5. Low Concentration Chemical Constituents Used in Test Solutions

Chemical	Concentration
$NaAlO_2$	0.5
Na_2CO_3	0.1
Na_2SO_4	0.1
Na_2HPO_4 x $7H_2O$	0.05
NaCl	0.1